ND-SR-PB ISOTOPE SYSTEMATICS OF THE JURASSIC KASSANDRA-SITHONIA OPHIOLITES AND CHORTIATIS MAGMATIC ARC SUITE, EASTERN VARDAR ZONE, NE GREECE

Nikolay Bonev*,✉ and **Massimo Chiaradia****

* *Department of Geology, Paleontology and Fossil Fuels, Sofia University, Bulgaria.*
** *Department of Earth Sciences, University of Geneva, Switzerland.*
✉ *Corresponding author, e-mail: niki@gea.uni-sofia.bg*

Keywords: *Nd-Sr-Pb isotopes; Kassandra-Sithonia ophiolites; Chortiatis arc; Vardar Zone; Greece.*

ABSTRACT

We report on the isotopic compositions of the intermediate rocks from Middle-Late Jurassic Chortiatis arc (160-173 Ma) and Kassandra-Sithonia back-arc ophiolites of Late Jurassic age (150-160 Ma), both exposed in the eastern Vardar Zone-western Circum-Rhodope belt transect of northeastern Greece. The Kassandra-Sithonia ophiolites consist of dunites, gabbros, basalts, and rhyolites, whose Nd-Sr-Pb isotopes are compatible with a dominant mantle-derived MORB component mixed with a detectable amount of crustal material and/or sediment entrained in their mantle source in a subduction zone. Their isotopic features are consistent with the origin of the studied rocks within the coupled Chortiatis arc/Kassandra-Sithonia back-arc system outboard the Eurasian continental margin (Serbo-Macedonian Massif). In both elements of the above-mentioned system, the documented Nd-Sr-Pb isotopes are comparable to those from the Middle Jurassic arc-related Evros ophiolites (164-176 Ma) in the eastern Circum-Rhodope belt of Bulgaria and Greece. This implies the presence of regionwide Vardarian Jurassic arc/back-arc systems connected with both western and the eastern Circum-Rhodope belts. A rhyolite dated at 149 Ma that intrudes the Sithonia ophiolite displays distinct Nd-Sr-Pb isotopic features suggesting an origin connected to a Late Jurassic-Early Cretaceous north-directed flat subduction zone within the Kassandra-Sithonia back-arc region, beneath the Eurasian continental margin. This subduction zone explains the granitoid magmatism (138-155 Ma) recorded along that margin to the north.

INTRODUCTION

Jurassic ophiolites mark the Vardar suture zone within the Alpine orogenic belt in the Aegean region of northern Greece (Fig. 1a). They are considered fragments of the oceanic lithosphere of the Neotethyan Vardar Ocean which finally closed in Paleocene times (e.g., Robertson and Dixon, 1984; Stampfli, 2000; Robertson, 2002; Stampfli and Hochard, 2009; Bortolotti et al., 2013). The Vardar Ocean had been limited by the Pelagonian and the Serbo-Macedonian-Rhodope continental margins and had developed intra-oceanic island arc-marginal basin systems during Jurassic times as highlighted by several tectonic models (e.g., Robertson et al., 1996; Stampfli and Borel, 2002; 2004; Bonev and Stampfli, 2003; Brown and Robertson, 2003; 2004; Schmid et al., 2008; Koglin et al., 2009; Papanikolaou, 2009; Robertson et al., 2013; Bonev et al., 2015a; 2015b). Both Serbo-Macedonian and Rhodope high-grade metamorphic basements are rimmed by a very low- to low-grade Circum-Rhodope Belt (CRB) that extends from the Chalkidiki Peninsula across the Aegean Sea to the Thrace region in northern Greece (Fig. 1a; Kauffmann et al., 1976): in these regions the western and eastern part of the CRB are exposed, respectively. The western CRB (see Fig. 1b, Peonias subzone) forms part of the eastern Vardar suture zone. The ophiolites of this area, exposed in the mainland Greece and in the Chalkidiki Peninsula of northern Greece (Fig. 1b), have been interpreted as formed in an ensialic oceanic back-arc basin (Bébien et al., 1987). In turn, the eastern CRB contains the unmetamorphosed arc-related, supra-subduction zone Evros ophiolite (e.g., Magganas et al., 1991; Magganas, 2002; Bonev and Stampfli, 2008; 2009), which has Early-Middle Jurassic magmatic ages (164-176 Ma) (Bonev et al., 2015a). Nd-Sr-Pb isotopes systematics demonstrate a record of crust-mantle interaction in the Evros ophiolite rock units (Bonev et al., 2023).

The south-vergent thrust system of the Rhodope and Serbo-Macedonian basements was constructed during a compressional phase in the hanging wall of a north-dipping Cretaceous-Tertiary subduction zone that was located within the Vardar Ocean to the south (Ricou et al., 1998). However, the Late Mesozoic convergence and thrusting phase was predated by intra-oceanic subduction that resulted in the formation of the eastern CRB Evros ophiolite, the eastern Vardar zone Kassandra-Sithonia ophiolites and the western CRB Chortiatis magmatic arc suite. These ophiolites, along with the associated Triassic-Jurassic sedimentary rocks, were thrust and accreted to the Serbo-Macedonian-Rhodope continental margin of Eurasia by Late Jurassic times (Bonev and Stampfli, 2003; 2011; Bonev et al., 2010; 2015a; Bonev and Filipov, 2018).

The very-low to low-grade CRB rocks form the uppermost metamorphic unit of the Rhodope and Serbo-Macedonian basements, with contrasting metamorphic grade and north-directed thrust and transpressional kinematics relative to the high-grade metamorphic basement (Bonev et al., 2010; Bonev and Stampfli, 2011; Bonev and Filipov, 2018). This indicates that along the eastern Vardar zone-western CRB transect and the eastern CRB transect, the low-grade rocks experienced a Late Jurassic deformational phase, becoming already part of the crustal architecture of the Alpine belt in the Balkan Peninsula by the earliest Cretaceous (Ivanova et al., 2015; Bonev et al., 2015a, 2015b). However, the nature of the melt source(s) of the eastern Vardar zone ophiolite-related gabbros, basalts and rhyolites, and associated arc-related diorites and granodiorites of the western CRB is not yet well understood. Nd and Sr isotope data suggest supra-subduction origin of the eastern Vardar zone ophiolitic crust (Chalkidiki and Kassandra-Sithonia inclusive) from a mantle source

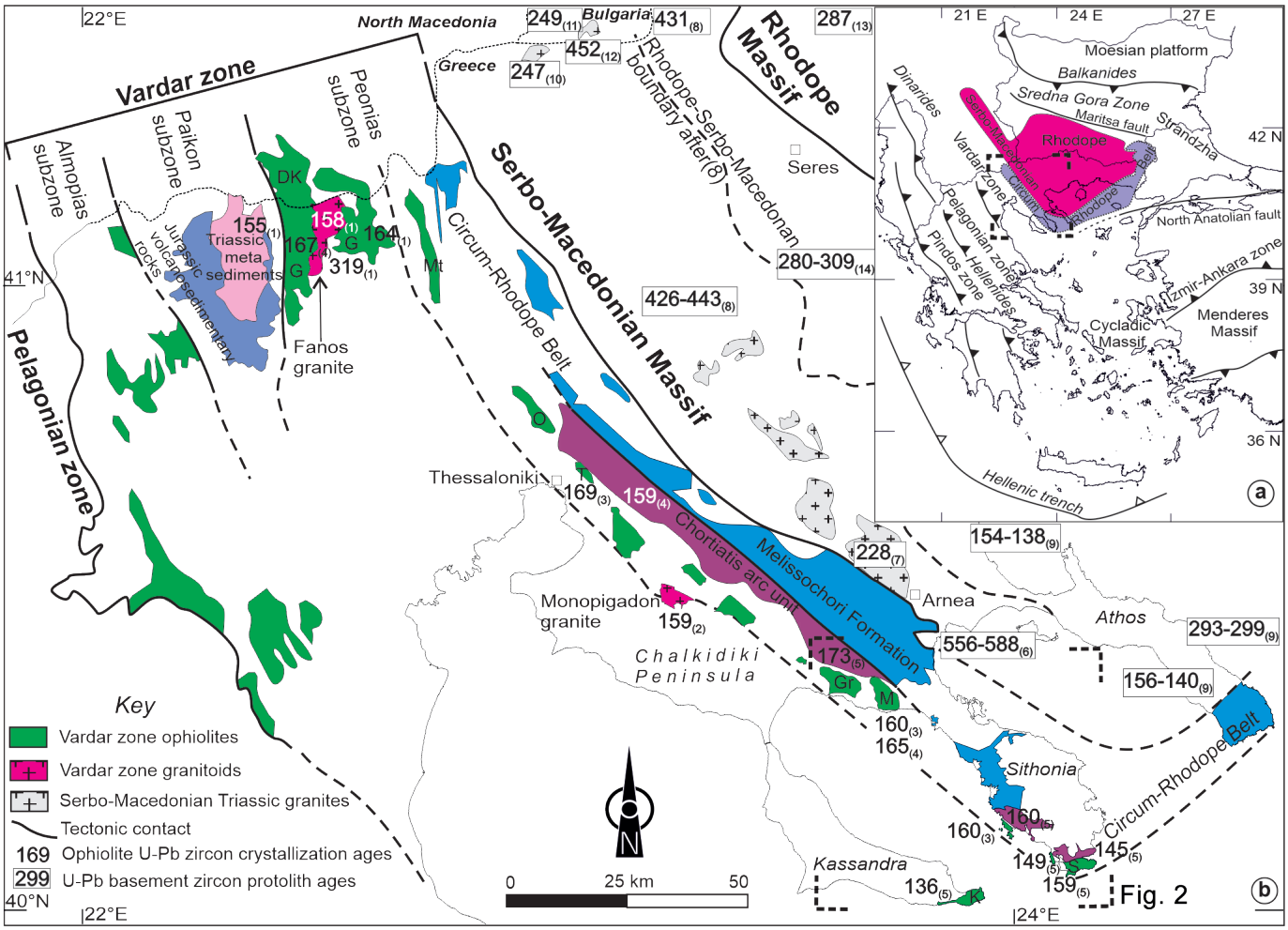

Fig. 1 - a) Alpine belt centered at the north Aegean region of the eastern Mediterranean, b) Tectonic map of the Vardar suture zone and adjacent units in the Internal Hellenides of northern Greece modified after Bonev et al., (2015b) who used data from Mercier (1966) and Kockel et al., (1977). Geochronology: 1, Anders et al., (2005); 2, Meinhold et al., (2009); 3, Zachariadis et al., (2006); 4, Zachariadis (2007); 5, Bonev et al., (2015b); 6, Himmerkus et al., (2006); 7, Himmerkus et al., (2009a); 8, Himmerkus et al., (2009b); 9, Himmerkus et al., (2012); 10, Christofides et al., (2007); 11, Macheva et al., (2006); 12, Peytcheva et al., (2005); 13, Turpaud and Reischmann (2010); 14, Himmerkus et al., (2007). Abbreviations of the ophiolite bodies: DK, Demir Kapija; G, Guevgueli; Gr, Gerakini; K, Kassandra; M, Metamorphosis; Mt, Metallikon; O, Oreokastro; S, Sithonia; T, Thessaloniki. The reader is referred to the PDF online for a colour version.

modified by an enriched component, likely subducted sediment (Zachariadis, 2007). The existing tectonic models consider the eastern Vardar zone-western CRB and the eastern CRB ophiolites formed in fore-arc, intra-arc/arc, and back-arc tectonic settings (Robertson et al., 1996; Robertson, 2002; Bonev and Stampfli, 2008; 2009; Saccani et al., 2008; 2011; Papanikolaou, 2009; Stampfli and Hochard, 2009; Bonev et al., 2010; Bortolotti et al., 2013; Bonev et al., 2015a; 2015b; Ferrière et al., 2016). These distinct arc-related environments have major implications for the subduction-accretion history of the Alpine belt in the Balkan Peninsula. Thus, the Jurassic crustal evolution needs to be validated with additional isotopic studies, particularly for the Kassandra-Sithonia ophiolites. The isotopic characteristics of the latter can be compared to that of the adjacent western CRB Chortiatis magmatic arc suite and the eastern CRB Evros ophiolite in order to obtain a regional-scale picture of the crustal build-up of the Alpine orogen along the Jurassic Eurasian plate margin.

In this paper, we present Nd-Sr-Pb radiogenic isotope geochemistry of gabbro, basalt and rhyolite from the Kassandra-Sithonia ophiolites and diorite and granodiorite from the Chortiatis continental magmatic arc in the eastern Vardar zone and western CRB, respectively, both exposed in northern Greece (Fig. 1b). Our results suggest crust (i.e. sediment)-mantle interaction for these rock units, which represent island arc/back-arc magmatic assemblages formed during the subduction evolution outboard of the Serbo-Macedonian margin in the Middle to Late Jurassic times. We first present an outline of the geology, geochemistry, and isotopic signature of the Jurassic Kassandra-Sithonia mantle-derived ophiolites and Chortiatis continental magmatic arc suite, and then discuss their origin in associated magmatic settings of the eastern Vardarian arc-back-arc system and their regional-scale significance.

GEOLOGICAL OUTLINE OF THE KASSANDRA-SITHONIA OPHIOLITES AND CHORTIATIS MAGMATIC ARC SUITE

In the Chalkidiki Peninsula of northern Greece, the main geological units exposed collectively along the branches of Kassandra and Sithonia are the following (Figs. 1b, 2; Kockel et al., 1977; Mussallam, 1991): (i) Neoproterozoic-Lower

Paleozoic (Himmerkus et al., 2006, 2009a) metamorphic basement of the Serbo-Macedonian Massif, which is intruded by Triassic rift-related granites (Himmerkus et al. 2009b) and also includes Triassic continental margin ophiolite (Bonev et al., 2019), (ii) Upper Triassic-Middle Jurassic metasedimentary rocks of the Svoula Formation (Kauffmann et al., 1976) or Melissochori Formation (Mercier, 1966) of the western CRB, (iii) the Jurassic Chortiatis magmatic suite of the western CRB (Kockel et al., 1977), (iv) Middle-Upper Jurassic ophiolites of the eastern Vardar zone (e.g., Spray et al., 1984) including the Kassandra-Sithonia ophiolites (Jung and Mussallam, 1985), (v) Upper Jurassic sedimentary rocks (Kockel et al., 1977; Jung and Mussallam, 1985), (vi) Lower Cretaceous limestone at Sithonia (Ivanova et al., 2015), (vii) the Eocene Sithonia granite (Christofides et al., 1990), and (viii) Neogene sedimentary rocks.

Because the Kassandra-Sithonia ophiolites associated with the Chortiatis magmatic suite are the subject of this study (Fig. 2), both units are described below. Details for other ophiolite occurrences in the Chalkidiki Peninsula and in the eastern Vardar zone can be found in Zachariadis (2007), Božović et al., (2013), Michail et al., (2016), and in Bonev and Filipov, (2018) for the western CRB units and in Kydonakis et al., (2016) and Bonev et al., (2019) for the Serbo-Macedonian Massif.

The Chortiatis magmatic suite (called also Chortiatis series, Kockel et al., 1977) consists of Na-rich diorites, quartz diorites, granodiorites, and granophyres metamorphosed to greenschist-facies that are intercalated with greenschist, phyllite, metachert, and marble. Field relations and stratigraphic correlations relative to the adjacent fossiliferous Svoula Formation of the western CRB (Kauffmann et al., 1976), led Kockel et al., (1977) to suggest that the Chortiatis magmatic suite encompasses the entire Jurassic period. Mussallam and Jung (1986a) have shown that the Chortiatis magmatic suite rock types have tholeiitic and mostly calc-alkaline affinity, and formed in an immature island arc setting. According to Mussallam and Jung (1986a), a pre-Tithonian deformation and greenschist-facies metamorphism is inferred for the Chortiatis magmatic suite. The tectonic contact between the Chortiatis magmatic suite and the Sithonia ophiolite is considered as a thrust fault along which the Chortiatis magmatic suite overrides the Sithonia ophiolite (Mussallam, 1991).

The Sithonia ophiolite (Jung and Mussallam, 1985) includes intrusive-extrusive crustal section of MORB-IAT, low K tholeiite to calc-alkaline gabbro, sheeted dykes, pillow and massive lavas, which formed in an oceanic rift tectonic environment. Based on similar MORB-IAT geochemical affinity, the Sithonia ophiolite has been correlated with the Kassandra ophiolite (Mussallam, 1991; Fig. 2). Jung and Mussallam (1985) assign the Sithonia ophiolite to the CRB, whereas Mussallam (1991) considers the Chortiatis magmatic suite as an island arc complex intruded by the sheeted dykes of the Sithonia ophiolite. In the southern tip of the Sithonia branch, platform-type limestone covering the Sithonia ophiolite revealed a Berriasian-early Valanginian biostratigraphic age

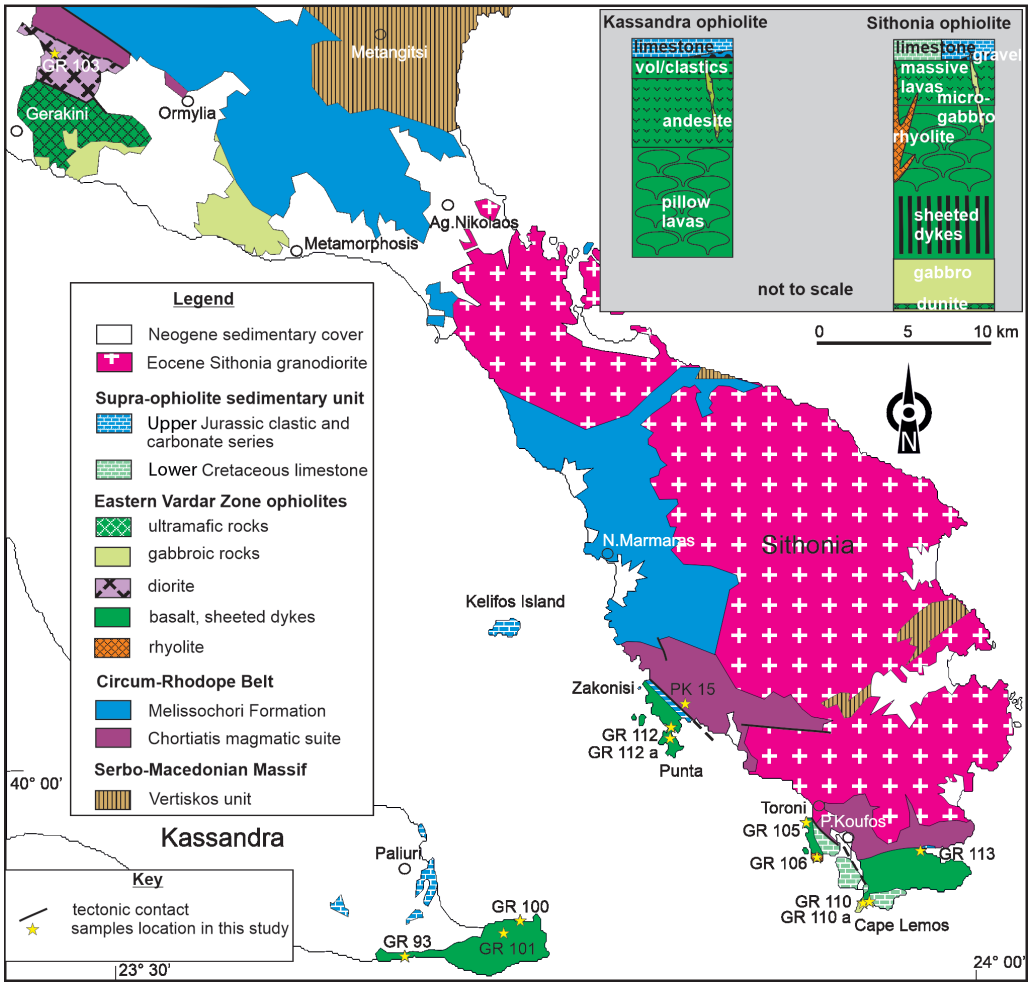

Fig. 2 - Geologic map of the Kassandra and Sithonia branches of the Chalkidiki Peninsula (modified after Bonev et al., (2015b) who used data from Kockel et al., (1977)). Locations and numbers of the samples investigated in this study are shown. The insert at top right shows a simplified columnar section derived from field observations of the ophiolites and supra-ophiolite sedimentary cover in Kassandra and Sithonia branches of the Chalkidiki Peninsula. The reader is referred to the PDF online for a colour version.

(Ivanova et al., 2015), that provides a minimum age limit for the magmatic evolution and emplacement history of the Sithonia ophiolite. The Eocene Sithonia granitoid pluton (51 Ma, Christofides et al., 1990) intrudes the Melissochori Formation and Chortiatis magmatic arc suite (Fig. 2).

Specifically, the Kassandra ophiolite section, together with its supra-ophiolite sedimentary cover rocks includes from the base to the top: (i) an upper crustal extrusive section of the Kassandra ophiolite, (ii) a volcanoclastic succession, (iii) carbonate rocks, and (iv) Neogene sedimentary rocks. The extrusive section of the Kassandra ophiolite consists of aphyric and pyroxene-phyric massive and pillow lavas. A single andesite dyke was emplaced at 136 Ma (Bonev et al., 2015b) into the overlying volcanoclastic succession, which recycles clasts from the Kassandra ophiolite. The volcanoclastic succession is separated into the Paliouri Formation (Feinberg et al., 1996; Michard et al., 1998) that overlies the Kassandra ophiolite.

In the southern part of the Kassandra branch, the Paliouri Formation is unconformably overlain by limestone that contains clasts from the Kassandra ophiolite lavas and volcanoclastic rocks. The limestone represents the basal horizon of the limestone exposed to the north which, in turn, is separated into the Xenia-Kelifos Formation (Michard et al., 1998). The latter formation is considered by authors as mentioned above analogous to the limestone exposed on Kelifos Island (see Fig. 2), where fossil findings provide a late Kimmeridgian biostratigraphic age for a similar limestone intercalated with pillow lavas (Mussallam and Jung, 1986a; Mussallam, 1991).

Neogene deposits represent sedimentary cover mainly consisting of sandstones that define a lateral discontinuity of the areal distribution of Jurassic ophiolites and supra-ophiolite sedimentary rocks at the Kassandra and Sithonia branches.

The eastern Vardar zone ophiolites and western CRB arc rocks have Middle to Late Jurassic magmatic crystallization ages ranging between 149 and 173 Ma (Spray et al., 1984; Smith, 1993; Anders et al., 2005; Zachariadis et al., 2006, 2007; Bonev et al., 2015b) (see Fig. 1b). The late subduction-related granitoids (i.e. Fanos and Monopigadon plutons, see Fig. 1b) intruded into the eastern Vardar zone ophiolites have magmatic crystallization ages of 158-159 Ma (Anders et al., 2005; Meinhold et al., 2009). The final magmatic pulse emplaced into the ophiolite is represented by late basalt and andesite dykes, and rhyolite body that fall in the age range of 136-149 Ma (Bonev et al., 2015b).

Therefore, a very good biostratigraphic and radiometric age control can be successfully exploited to obtain the significance of isotopic systematics of the studied eastern Vardar zone ophiolites and western CRB arc rocks for deciphering mantle and crustal processes involved in the subduction-accretion history.

WHOLE-ROCK GEOCHEMISTRY

Whole-rock geochemical compositions of several samples studied here for radiogenic isotopes (GR93, GR103, GR106, GR110, GR112, GR113) have been published and discussed in Bonev et al., (2015b) (Table 1). Here, we add to them the geochemical compositions of another set of samples (GR100, GR101, GR105, GR110a, GR112a, PK15) and briefly discuss their trace elements characteristics. All the available analyses are reported in Table 2.

Rb and Ba shows slightly variable concentrations as SiO_2 contents increase; their concentrations are high in evolved samples such as andesite and rhyolite due to magmatic fractionation processes, as well as in the sheeted dykes where fluid circulation is documented along the contacts (Bonev et al., 2015b) (Fig. 3a-c). Sr and Nb concentrations at increasing SiO_2 content exhibit nearly linear trend, except for the rhyolite sample (Fig. 3b-d). We consider the above trace elements characteristics as reflecting primary magmatic signature of the studied samples and, at al lesser extent, an ocean-floor hydrothermal processes.

Chondrite-normalized REE compositions of the Kassandra-Sithonia rock samples generally exhibit middle and heavy REE flat patterns, similar to N-MORB and E-MORB that deviate to progressive light REE enrichment relative to N-MORB and E-MORB (Fig. 3e). The chondrite-normalized REE profile of rhyolite shows a strongly fractionated pattern, having the highest LREE-enrichment compared to the ophiolite samples, coupled with a significant heavy REE-depletion relative to N-MORB and E-MORB compositions. The dunite and one basalt sample display the strongest REE-depletion relative to N-MORB and E-MORB compositions. The Chortiatis magmatic arc diorite has a chondrite-normalized REE profile that broadly parallels the profiles of the Kassandra-Sithonia ophiolites samples but, compared to them, the diorite exhibits 10-20 times higher REE abundances.

N-MORB normalized multi-element profiles of all samples display high ratios of large-ion lithophile elements (LILE) and high-field strength elements (HFSE) (Fig. 3f). Negative Nb anomaly characterizes the majority of the Kassandra-Sithonia ophiolitic rock samples, with exceptions of the depleted dunite and basalt samples mentioned above. All samples (except Chortiatis arc diorite and Kassandra dyke) also show variably negative Ba, Ce, Ti and P anomalies that indicate involvement of feldspar, apatite and Fe-Ti oxides in magma fractionation processes. Pronounced positive Th and Pb anomalies characterize all studied samples. In terms of HFSE, and middle and heavy REE, the majority of the Kassandra-Sithonia ophiolites samples have concentrations close to N-MORB or slightly depleted whereas they significantly overlap E-MORB composition. Relative to HFSE and HREE the Chortiatis arc diorite exhibits distinctly higher concentrations compared to the Kassandra-Sithonia ophiolitic rocks. All studied samples depart significantly from the oceanic island basalt (OIB) composition in chondrite- and N-MORB-normalized diagrams (Fig. 3e-f).

ND-SR-PB ISOTOPES

Methods

Chemical separation of the elements from whole rocks and isotopic analyses were performed at the Department of Earth Sciences at University of Geneva (Switzerland). Nd-Sr-Pb isotopes were measured with a Thermo Neptune PLUS Multi-Collector ICP-MS. For monitoring the internal fractionation, we used $^{88}Sr/^{86}Sr = 8.375209$ for the $^{87}Sr/^{86}Sr$ ratio, $^{146}Nd/^{144}Nd = 0.7219$ for the $^{143}Nd/^{144}Nd$ ratio and $^{203}Tl/^{205}Tl = 0.418922$ for the three Pb ratios. Long-term reproducibility of the measurements was controlled by repeated measurements of the external standards SRM987 ($^{87}Sr/^{86}Sr = 0.710248$, McArthur et al., 2001), JNdi-1 ($^{143}Nd/^{144}Nd = 0.512115$, Tanaka et al., 2000), and SRM981 (Baker et al., 2004) for Pb (see Table 1S). Additional details on analytical procedures can be found in Chiaradia et al., (2020). Whole-rock Nd, Sr, and Pb isotopic compositions are listed in Table 3. The Nd-Sr-Pb isotopic results were age-corrected to the

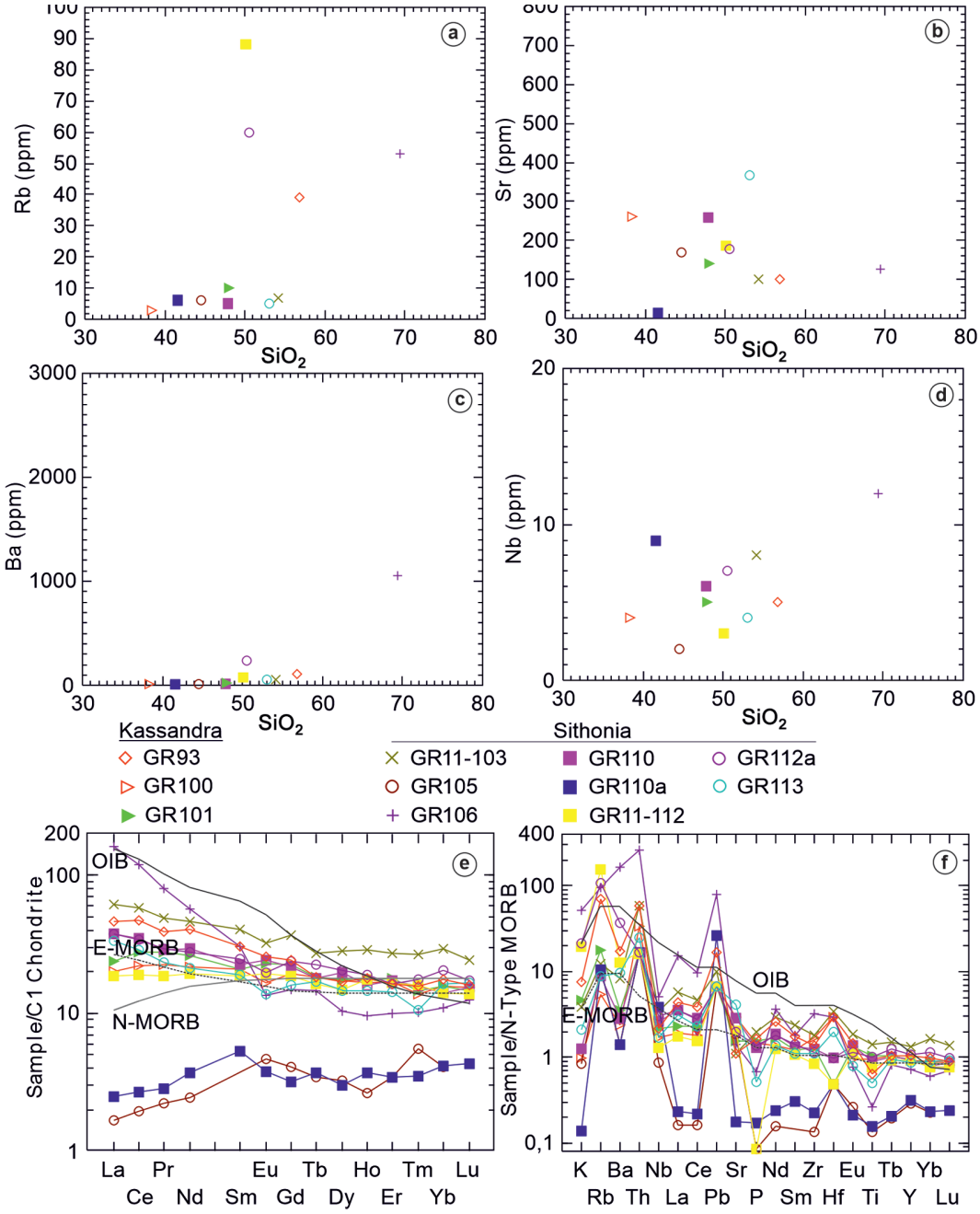

Fig. 3 - Trace elements and rare-earth elements patterns of studied rocks in the Kassandra-Sithonia ophiolites and Chortiatis arc diorite. Diagrams in a), b), c) and d) show the covariation of SiO_2 and Rb, Sr, Ba and Nb (ppm), respectively, e) chondrite-normalized diagram, f) N-MORB normalized spider diagram. Normalization values, N-MORB, E-MORB and OIB compositions after Sun and McDonough (1989). The reader is referred to the PDF online for a colour version.

known crystallization ages of the Kassandra and Sithonia ophiolites or biostratigraphic age of the sedimentary rocks associated with these ophiolites and known crystallization ages for the Chortiatis magmatic arc suite (see Table 1).

Results

We have analyzed Nd, Sr and Pb isotopic compositions of three samples from the Kassandra ophiolitic basalt and andesite and seven samples from the Sithonia ophiolite dunite, gabbro, basalt and rhyolite, together with two samples - diorite and granodiorite from the intrusive section of the Chortiatis magmatic arc suite (Fig. 2, see Table 1). Nd, Sr and Pb isotope results have been compared with published Nd and Pb isotopic compositions of the ophiolitic rocks in the Mandritsa unit of the eastern CRB in Bulgaria (Bonev and Stampfli, 2008) and Nd, Sr and Pb isotopes from the Evros ophiolite in Greece (Bonev et al., 2023), together with available Nd and Sr isotopic compositions for the Kassandra-Sithonia ophiolites (Zachariadis, 2007).

The $^{143}Nd/^{144}Nd$ ratios of the dunite, gabbro, diorite, granodiorite, basalts, andesite and rhyolite rock samples fall in the range of 0.512377-0.512923, with positive $\varepsilon_{Nd\ (CHUR)}$ values that are characteristic of mantle-derived melts. Only the rhyolite sample GR106 (ε_{Nd} = -5.1) and the andesite sample GR93 (ε_{Nd} = -0.2) display negative ε_{Nd} values. When time-corrected for the crystallization age of the mafic rocks (150 Ma to 173 Ma, see Table 1), the $\varepsilon_{Nd(t)}$ values vary from +0.2 to +6.0 (Table 3).

The $^{87}Sr/^{86}Sr$ ratios display values ranging from 0.704306 to 0.706820 that are characteristic of the oceanic crust and subduction-related volcanic rocks. However, a rhyolite sample GR106 at Sithonia has a higher $^{87}Sr/^{86}Sr$ value of 0.708353.

Table 1- Summary of studied samples from the Kassandra-Sithonia ophiolites and Chortiatis magmatic arc suite.

Sample	Rock type	Remark	Age	Location
GR93	andesite	dyke emplaced into volcanoclastic succession of Paliuri Formation	U-Pb zircon age 136.3 ± 1.86 Ma (Bonev et al., 2015b)	Kassandra
GR100	basalt	pillow lava	150 Ma based on intercalation with Kimmeridgian limestone on Kelifos Island (Mussallam, 1991)	Kassandra
GR101	basalt	pillow lava	150 Ma based on intercalation with Kimmeridgian limestone on Kelifos Island (Mussallam, 1991)	Kassandra
GR103	diorite	massive	U-Pb zircon age 172.76 ± 1.2 Ma (Bonev et al., 2015b)	Gerakini, Sithonia
GR105	basalt	massive lava	150 Ma based on nearby cross-cutting rhyolite with an age of 148.9 ± 1.0 Ma (Bonev et al., 2015b)	Toroni, Sithonia
GR106	rhyolite	massive, emplaced into massive and pillow lavas	U-Pb zircon age 148.9 ± 1.0 Ma (Bonev et al., 2015b)	Toroni, Sithonia
GR110	gabbro	isotropic and layered	U-Pb zircon age 158.4 ± 1.0 Ma	Cape Lemos, Sithonia
GR110a	dunite	layer emplaced into the Cape Lemos gabbro	159 Ma based on the age of the Cape Lemos gabbro	Cape Lemos, Sithonia
GR112	basalt	sheeted dyke	160 Ma based on the U-Pb zircon age 160 ± 1.2 Ma (Zachariadis, 2007)	Punta, Sithonia
GR112a	basalt	sheeted dyke	160 Ma based on the U-Pb zircon age 160 ± 1.2 Ma (Zachariadis, 2007)	Punta, Sithonia
GR113	basalt	dyke emplaced into Kimmeridgian conglomerate (e.g. Mussallam, 1991)	U-Pb zircon age 144.6 ± 3.14 Ma (Bonev et al., 2015b)	Sithonia
PK15	granodiorite	massive, emplaced into Chortiatis arc metavolcanic rocks (greenschist)	U-Pb zircon age 159.6 ± 0.60 Ma (Bonev and Filipov, 2018)	Sithonia

Sample locations are shown in Fig. 2; whole-rock composition are reported in Bonev et al. (2015b).

These results indicate that the analyzed mafic rocks originated from magmas that were derived from a similar mantle source with a high time-integrated Sm/Nd ratio and a moderate to slightly elevated range of Rb/Sr ratios. When plotted in the $^{143}Nd/^{144}Nd$ vs. $^{87}Sr/^{86}Sr$ diagram (Fig. 4a), the majority of the samples fall within and parallel to the mantle array and plot close to the Bulk Silica Earth (BSE), while samples GR93, GR112 and GR112a plot at higher $^{87}Sr/^{86}Sr$ values. Because these samples come from dykes, some sea-water alteration is expected similar to that described by Bonev et al. (2015) for the dyke contacts, which provide an explanation of the higher $^{87}Sr/^{86}Sr$ isotope values.

The analyzed rocks show a relatively narrow range of $^{206}Pb/^{204}Pb$ (18.212-19.483) and $^{207}Pb/^{204}Pb$ (15.435-15.698) ratios and a relatively narrow range of $^{208}Pb/^{204}Pb$ values (38.104-39.368), reaching a higher value in sample GR113 (Table 3). Almost all studied rocks exhibit a linear trend parallel to progressive enrichment along the MORB-oceanic island basalt (OIB) line in the $^{207}Pb/^{204}Pb$-$^{206}Pb/^{204}Pb$ correlation diagram (Fig. 4d), plotting above the Northern Hemisphere Reference Line (NHRL) where enriched mantle reservoirs (EMI, EMII) are identified (Zindler and Hart, 1986). An exception of Pb isotopic compositions are dunite sample GR110a and dyke sample GR113 plotting respectively within the MORB and OIB fields (Rollinson, 1993). In the $\varepsilon_{Nd,i}$ vs. $^{206}Pb/^{204}Pb$ diagram, samples show nearly linear trend towards higher $\varepsilon_{Nd,i}$ values plotting between MORB and BSE (Fig. 4e). In a $^{143}Nd/^{144}Nd$ vs. $^{206}Pb/^{204}Pb$ diagram isotopic ratios cluster between the BSE, Prevalent Mantle (PREMA) and Mid-Ocean Ridge Basalt (MORB) (Fig. 4b) and spread along the same mantle reservoirs towards higher $^{87}Sr/^{86}Sr$ values in the $^{87}Sr/^{86}Sr$ vs. $^{206}Pb/^{204}Pb$ diagram (Fig. 4c).

The analyzed Kassandra-Sithonia ophiolites have Pb isotope ratios that cluster closely with those of the Jurassic gabbro and basalts of the Evros ophiolite (Bonev et al., 2023), as well as with those of the Mandritsa unit of the CRB in Bulgaria,

Table 2 - Whole-rock geochemical data for the studied samples from the Kassandra-Sithonia ophiolites and Chortiatis magmatic arc suite.

Sample	GR93	GR100	GR101	PK15	GR103	GR105	GR106	GR110	GR110a	GR112	GR112a	GR113
Rock type	and	bas	bas	gd	d	bas	rhy	gb	dun	bas	bas	bas
Location	KAS	KAS	KAS	SIT	SIT	SIT	SIT	SIT	SIT	SIT	SIT	SIT
SiO_2	56.82	38.31	48.07	62.24	54.13	44.54	69.38	47.91	41.55	50.08	50.46	53.09
TiO_2	0.82	1.22	1.34	0.65	1.79	0.17	0.34	1.12	0.20	0.98	1.28	0.64
Al_2O_3	14.26	12.72	15.63	16.75	14.61	14.89	14.85	14.28	3.48	15.30	14.92	19.10
$Fe_2O_{3\ (tot)}$	11.73	7.85	9.33	6.42	12.53	6.54	2.69	8.56	13.33	9.38	11.01	7.42
MnO	0.23	0.16	0.14	0.06	0.21	0.11	0.04	0.13	0.14	0.17	0.18	0.18
MgO	4.32	3.84	7.27	2.32	3.51	14.47	1.13	7.00	26.27	8.25	6.98	2.78
CaO	2.81	18.11	9.04	3.55	5.21	13.80	0.94	10.96	6.50	9.99	7.43	10.57
Na_2O	2.72	3.65	3.66	5.04	5.18	0.33	4.84	3.82	n.d.	1.78	2.74	4.20
K_2O	0.54	0.07	0.34	0.27	0.28	0.06	3.72	0.09	0.01	1.42	1.56	0.15
P_2O_5	0.19	0.17	0.18	0.10	0.23	0.01	0.08	0.15	0.02	0.10	0.16	0.06
Cr_2O_3	n.d.	0.03	0.03	n.d.	n.d.	0.05	n.d.	0.07	0.32	0.04	n.d.	n.d.
NiO	n.d.	0.01	0.01	n.d.	n.d.	0.03	n.d.	0.02	0.11	0.01	n.d.	n.d.
LOI	4.68	13.14	3.98	2.44	1.50	4.23	1.10	5.12	7.33	1.76	2.62	1.04
Total	99.13	99.28	99.01	99.85	99.17	99.21	99.10	99.25	99.26	99.26	99.32	99.22
Nb	5	4	5	2	8	2	12	6	9	3	7	4
Ta	0.18	0.23	0.17	0.22	0.37	n.d.	2.62	0.22	n.d.	0.10	0.24	0.20
Zr	101	125	96	79	132	10	242	93	17	63	84	83
Y	29	26	26	21	37	8	20	27	9	26	30	24
Cs	0.38	n.d.	0.50	0.28	0.36	0.22	0.32	0.37	2.75	1.50	0.77	0.28
Rb	39	3	10	6	7	6	53	5	6	88	60	5
Sr	100	261	140	386	101	169	126	258	16	186	179	366
Ba	107	15	22	66	53	<9	1051	18	<9<	81	236	60
U	5	2	2	5	3	<2	11	<2	<2	<2	<2	2
Th	7	4	<2	5	7	<2	31	<2	<2	<2	<2	3
Pb	5	<2	<2	29	3	<2	24	<2	8	<2	<2	<2
Hf	6	6	<1	1	7	<1	6	2	<1	<1	2	4
Sc	22	<2	45	15	48	39	4	37	98	37	50	28
Cr	5	289	247	21.34	7	364	14	502	1646	263	24	19
V	41	244	283	117	397	122	48	269	129	254	307	274
Ni	<2	74	84	<8.50	4	172	8	168	691	67	31	12
Ga	16	15	18	17.13	20	11	16	17	7	16	18	19
Zn	72	83	70	18.64	76	41	36	73	67	55	97	35
Cu	<2	62	39	<1.58	6	25	9	55	68	73	39	4
Co	9	34	38	7.77	39	53	21	44	123	40	41	21
La	10.98	4.74	5.68	9.73	14.48	0.40	38.55	8.96	0.59	4.39	8.87	7.90
Ce	28.86	13.51	17.10	21.72	35.38	1.20	72.68	21.51	1.65	11.64	21.03	17.54
Pr	3.72	2.13	2.64	2.69	4.66	0.21	7.63	2.75	0.27	1.77	2.80	2.22
Nd	18.89	10.80	12.34	12.22	21.58	1.15	26.73	13.65	1.74	9.08	13.05	9.90
Sm	4.65	3.22	3.22	3.44	6.26	n.d.	4.71	3.47	0.82	2.86	3.76	2.89
Eu	1.49	0.97	1.34	0.80	1.88	0.27	0.79	1.42	0.22	1.13	1.15	0.80
Gd	5.03	3.97	4.63	3.23	7.58	0.84	3.04	4.43	0.66	3.84	4.86	3.26
Tb	0.69	0.69	0.69	0.56	1.02	0.13	0.54	0.67	0.14	0.61	0.85	0.64
Dy	4.32	4.38	4.50	3.73	7.12	0.83	2.65	5.05	0.76	3.78	5.18	3.72
Ho	1.01	0.94	0.97	0.75	1.64	0.15	0.54	0.90	0.21	0.99	1.08	0.82
Er	2.72	2.78	2.95	2.36	4.49	0.57	1.66	2.85	0.57	2.73	2.72	2.36
Tm	0.40	0.35	0.37	0.33	0.68	0.14	0.26	0.40	0.09	0.41	0.45	0.27
Yb	2.98	2.69	2.66	2.27	4.96	0.70	1.86	2.40	0.71	2.38	3.50	2.76
Lu	0.41	0.39	0.37	0.33	0.62	n.d.	0.32	0.39	0.11	0.35	0.44	0.42

Major elements (wt%) and trace elements (ppm) analysed by XRF. REE +Ta, Cs (ppm) analysed by LA-ICP-MS. n.d. = not detected.
Abbreviations: and, andesite; bas, basalt; d, diorite; gb, gabbro; gd, granodiorite; rhy, rhyolite. Locations: KAS, Kassandra, SIT, Sithonia.

Table 3 - Nd, Sr and Pb isotopic compositions of the Kassandra-Sithonia ophiolites and Chortiatis magmatic arc suite rocks

Sample	GR93	GR100	GR101	GR103	GR105	GR106	GR110	GR110a	GR112	GR112a	GR113	PK15
Measured ratio												
$^{143}Nd/^{144}Nd$	0.512606	0.512922	0.512892	0.512683	0.512752	0.512353	0.512793	0.512899	0.512876	0.512774	0.512623	0.512710
1SE	0.000003	0.000003	0.000003	0.000002	0.000013	0.000001	0.000002	0.000011	0.000003	0.000002	0.000003	0.000002
^{140}Ce	1.322	1.319	0.816	1.218	0.036	9.003	1.949	0.054	0.594	1.144	2.867	2.676
^{144}Nd signal	1.644	1.117	1.643	2.52	0.139	5.401	2.152	0.144	1.466	2.316	1.141	1.628
$^{87}Sr/^{86}Sr$	0.706787	0.704319	0.704563	0.705786	0.704320	0.708367	0.706065	0.704595	0.706834	0.706711	0.706017	0,705996
1SE	0.000007	0.000003	0.000006	0.000008	0.000005	0.000007	0.000005	0.000024	0.000006	0.000006	0.000004	0.000004
^{86}Sr	0.200	0.670	0.310	0.170	0.410	0.210	0.410	0.040	0.270	0.270	0.530	0.580
^{86}Sr signal	1.79	5.85	2.75	1.51	3.58	1.82	3.60	0.36	2.39	2.39	4.66	5.11
1σ (ppm)	0.001759	0.000839	0.001347	0.001957	0.011410	0.001739	0.001137	0.004800	0.001468	0.001467	0.000967	0.000913
1σ ppm (ext.uncert.)	0.000012	0.000006	0.000009	0.000014	0.000008	0.000012	0.000008	0.000034	0.000010	0.000010	0.000007	0.000006
$^{208}Pb/^{204}Pb$	38.9424	38.1208	38.2337	39.1788	38.5518	39.0785	38.7682	38.0485	38.7479	38.9304	39.3111	38.8953
$^{207}Pb/^{204}Pb$	15.6734	15.5329	15.5188	15.6761	15.6305	15.6810	15.6232	15.4188	15.6143	15.6463	15.6452	15.6464
$^{206}Pb/^{204}Pb$	19.0991	18.1986	18.4273	19.0372	18.5717	18.8810	18.6683	18.3371	18.6535	18.9491	19.4686	18.9377
1SE6/4	0.0023	0.0030	0.0061	0.0023	0.0031	0.0005	0.0039	0.0174	0.0103	0.0064	0.0060	0.0019
1SE7/4	0.0019	0.0027	0.0052	0.0015	0.0025	0.0004	0.0033	0.0147	0.0086	0.0041	0.0049	0.0015
1SE8/4	0.0047	0.0064	0.0127	0.0041	0.0063	0.0011	0.0079	0.0358	0.0213	0.0112	0.0120	0.0038
^{208}Pb	0.3188	0.2051	0.1058	0.4064	0.2394	1.7118	0.1685	0.0371	0.0668	0.1559	0.1179	0.1179
^{205}Tl	1.2680	1.2767	1.3161	1.2073	1.1576	1.2009	1.2061	1.2262	1.2059	1.2057	1.2449	1.1974
Age corrected ratio (Ma)	136.3 Ma	150 Ma	150 Ma	172.8 Ma	150 Ma	148.9 Ma	158.4 Ma	158.4 Ma	160 Ma	160 Ma	144.6 Ma	159.6 Ma
$^{143}Nd/^{144}Nd_i$	0.512630	0.512946	0.512916	0.512707	0.512776	0.512377	0.512817	0.512923	0.512900	0.512798	0.512647	0.512734
εNd_i	-0.2	6.0	5.4	1.3	2.7	-5.1	3.5	5.6	5.1	3.1	0.2	1.9
$^{87}Sr/^{86}Sr_i$	0.706773	0.704306	0.704549	0.705772	0.704306	0.708353	0.706051	0.704581	0.706820	0.706697	0.706004	0.705982
$^{208}Pb/^{204}Pb$	38.999	38.176	38,289	39.235	38.608	39.135	38.824	38.104	38.804	38.987	39.368	38.952
$^{207}Pb/^{204}Pb$	15.690	15.550	15.536	15.693	15.647	15.698	15.640	15.435	15.631	15.663	15.662	15.663
$^{206}Pb/^{204}Pb$	19.113	18.212	18.441	19.051	18.585	18.895	18.682	18.350	18.667	18.963	19.483	18.951

Values corrected for internal fractionation using $^{88}Sr/^{86}Sr=8.375209$ and for external fractionation using a nominal value of SRM987 $^{87}Sr/^{86}Sr=0.710248$ (McArthur et al., 2001).
Values corrected for internal fractionation using $^{146}Nd/^{144}Nd=0.7219$ and for external fractionation using a nominal value of JNdi1 $^{143}Nd/^{144}Nd=0.512115$ (Tanaka et al., 2000).
Values corrected for internal fractionation using $^{203}Tl/^{205}Tl=0.418922$ and for external fractionation using nominal values of SRM981 of Baker et al. (2004).

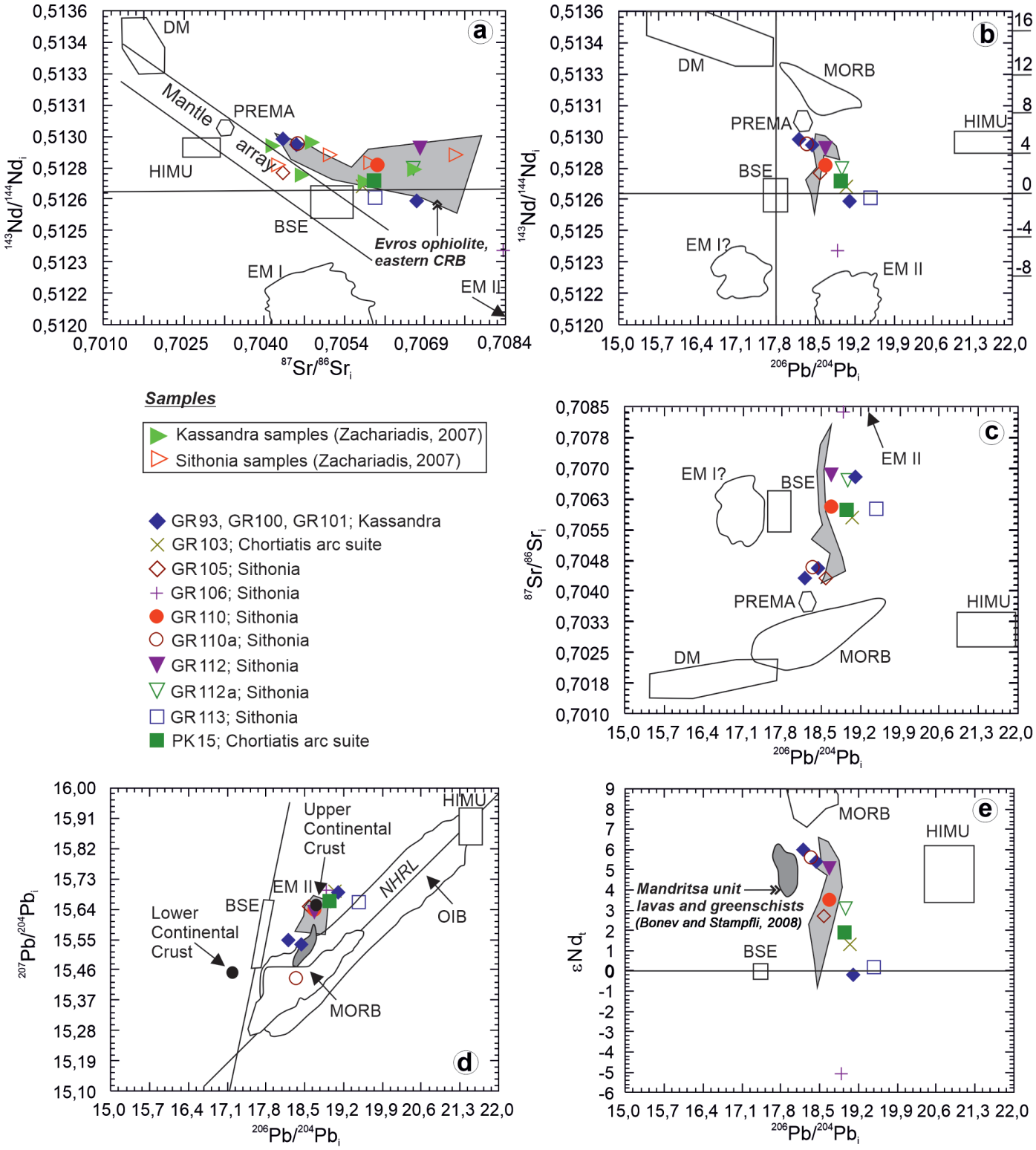

Fig. 4 - Correlation diagrams for Nd-Sr-Pb isotopes of the studied rocks from the Kassandra-Sithonia ophiolites and Chortiatis mgmatic arc suite. a) $^{143}Nd/^{144}Nd$ vs. $^{87}Sr/^{86}Sr$ diagram. DMM (Depleted MORB Mantle), EM I and EM II mantle reservoirs from Hart (1984), b) $^{143}Nd/^{144}Nd$ vs. $^{206}Pb/^{204}Pb$ diagram, c) $^{87}Sr/^{86}Sr$ vs. $^{206}Pb/^{204}Pb$ diagram, d) $^{207}Pb/^{204}Pb$ vs. $^{206}Pb/^{204}Pb$ diagram, e) $\varepsilon_{Nd,i}$ vs. $^{206}Pb/^{204}Pb$ diagram. Shaded field of Nd-Pb isotopes of Mandritsa unit is from Bonev and Stampfli (2008), and the field of Nd-Sr-Pb isotopes for Evros ophiolite is from Bonev et al. (2023). The NHRL and the fields of reference mantle reservoirs are after Zindler and Hart (1986), and the fields of OIB and MORB from Rollinson (1993). The reader is referred to the PDF online for a colour version.

which are also Jurassic (Bonev and Stampfli, 2008). These isotopic signatures partly plot within the OIB (Ocean Island Basalt) field, closest to the MORB (Mid-Ocean Ridge Basalt) field (Fig. 4 d-e). The Nd and Sr isotope ratios of the studied samples demonstrate a remarkable overlapping with the Nd and Sr isotope ratios for the Kassandra-Sithonia ophiolites previously reported by Zachariadis (2007), as well as with the same ratios documented for the Evros ophiolite (Bonev et al., 2023) (Fig. 4a-b). Overall, when the Jurassic Kassandra-Sithonia ophiolites are compared to Jurassic Evros ophiolite

and Mandritsa unit samples, both ophiolite suites together with the Jurassic Chortiatis arc suite rocks display striking similarities in terms of Nd-Sr-Pb isotopic compositions (Fig. 4). However, the rhyolite sample GR106 has Nd-Sr-Pb isotopic compositions distinct from ophiolite above and arc units.

DISCUSSION AND CONCLUSIONS

The Nd isotope compositions obtained in this study are consistent with involvement of MORB-like reservoir, a compositional feature also displayed by trace element and REE geochemistry of the studied samples from the Kassandra-Sithonia ophiolites, which were formed at a back-arc spreading center (Bonev et al., 2015b; Fig. 4). The range of Nd isotopes is consistent with the values of the oceanic crust formed in the seafloor and in arc-related settings from a mantle peridotite. This is also valid for the Chortiatis arc magmatic suite samples which have Nd isotopic composition overlapping or close to the samples of the Kassandra-Sithonia ophiolites (Fig. 4a-c). The Pb isotope data also suggest a contribution of a MORB mantle source (Fig. 4b-d). The relatively narrow range of $\varepsilon_{Nd,i}$ and Pb isotope values indicates that the mantle source of the basalts, gabbro and dunite was a rather homogenous depleted MORB-type lithospheric mantle (Fig. 4).

The range of Sr isotopes also supports a MORB-type mantle component in the source region, but additionally shows an enrichment process via crustal contamination. This explains the variations and relatively high 87Sr/86Sr ratio observed in samples GR112a, GR112, and GR93. We infer a contribution from continental crust to explain the elevated $^{87}Sr/^{86}Sr$ ratios (respectively 0.7066, 0.7067 and 0.7068) observed in these samples. This interpretation is compatible with the inherited Paleozoic zircon clusters in samples GR93 and GR112 (Bonev et al., 2015b). However, the slightly negative $\varepsilon_{Nd,i}$ value of sample GR93 suggests the involvement of subducted sediments in the magma genesis. Because samples GR93, GR112, GR112a belong to the back-arc segment, their $^{87}Sr/^{86}Sr$ values could

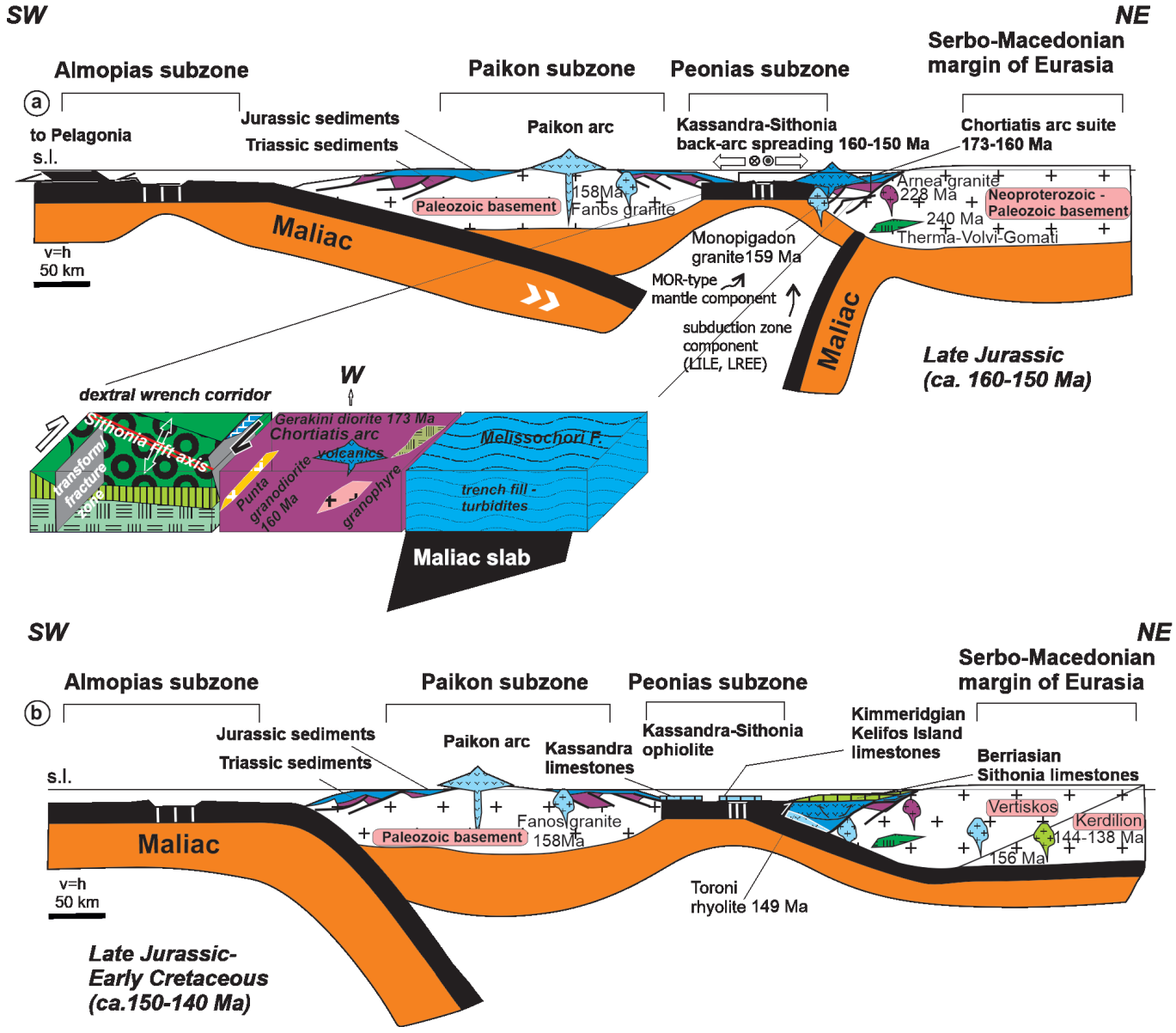

Fig. 5 - Simplified tectonic model of Late Jurassic-Early Cretaceous Chortiatis arc/Sithonia back-arc system development in the eastern Vardar zone. Modified after Bonev et al.(2015b) and Bonev and Filipov (2018). The reader is referred to the PDF online for a colour version.

demonstrate a sedimentary input into the back-arc mantle region from the subduction zone responsible for the formation of the Chortiatis magmatic arc. These Sr isotopic features are similar to previously documented Sr isotopes for the Kassandra-Sithonia ophiolites and compatible with their mantle source interpretation involving subducted sedimentary rocks (Zachariadis, 2007). This sedimentary contribution to the mantle source is further evidenced by the elevated Pb isotopes ratios of some of the Kassandra-Sithonia ophiolite samples that show similarity to those of the Chortiatis magmatic arc suite (Fig. 4d). We infer, therefore, the involvement of a MORB-type mantle mixed with a crustal component, presumably subducted sediments, in the mantle source of the subduction zone for the Chortiatis magmatic arc-Kassandra-Sithonia back-arc system (Fig. 5a).

However, the rhyolite melt represented by the sample GR106 had a different origin, as supported by Nd-Sr-Pb isotope data. As previously proposed (Bonev et al., 2015b), we suggest that the Monopigadon granite and Toroni rhyolite represent mid- to shallow crustal level differentiates likely resulting from a flat N-directed subduction initiated within the Kassandra-Sithonia back-arc region. This subduction also explains the origin of the granitoids and metagranitoids of similar age and their occurrences within the Eurasian continental margin, i.e., the Serbo-Macedonian Massif further north (Fig. 5b).

Our results highlight coherent Nd-Sr-Pb isotopic ratios for the Kassandra-Sithonia ophiolites and Chortiatis magmatic arc suite, indicating generation of magmas by partial melting of a MORB-type mantle source. These isotopic data indicate variable contamination of magmas by continental crust material and/or sedimentary rocks entrained in the subduction zone (Fig. 4). Comparison of the obtained Nd-Sr-Pb isotope results with analogous data from the Evros ophiolite mafic rocks demonstrates regionwide similarity of the isotopic compositions (Fig. 4), which in turn provides additional support for the involvement of time-integrated analogous source mantle in the arc/back-arc systems, in both eastern Vardar zone-western CRB segment and eastern CRB in the Tethyan realm. Indeed, if we restore the pre-Oligocene rotation in the north Aegean region (e.g., Bonev and Stampfli, 2010; Bonev et al., 2015b), coherent ages and Nd-Sr-Pb isotopic compositions both imply a regionally extensive Middle-Late Jurassic arc/back-arc systems represented by Evros arc-related ophiolite-back-arc Samothraki ophiolite, and the Chortiatis magmatic arc-Kassandra-Sithonia back-arc ophiolites (Fig. 6).

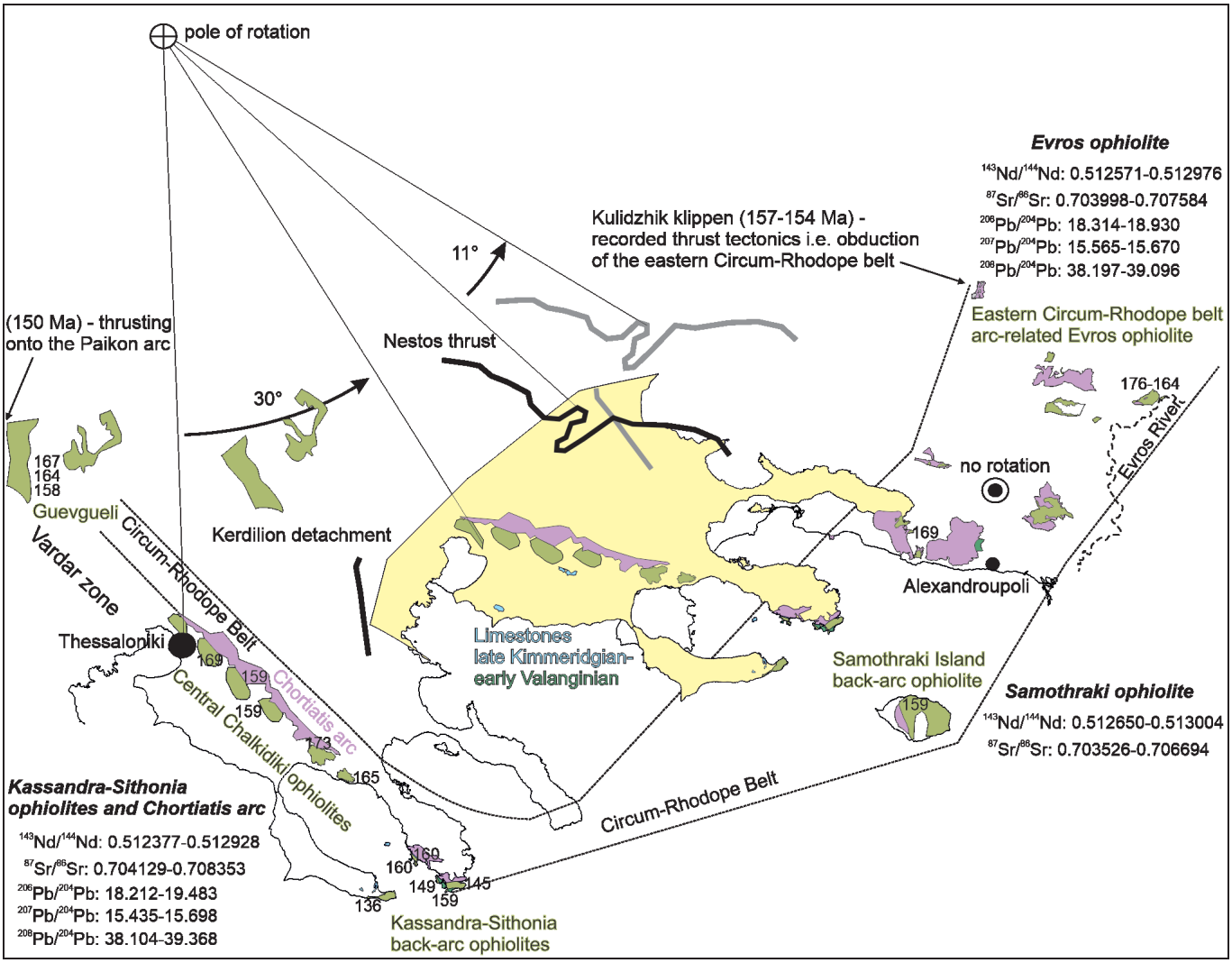

Fig. 6 - Age distribution of the Jurassic ophiolites along the eastern Vardar zone-Circum-Rhodope belt transect in the north Aegean region (modified after Bonev and Stampfli (2010) using the base and pole of rotation from Brun and Sokoutis (2007)). The isotope data adapted in the light of published by Zachariadis (2007) for Kassandra-Sithonia ophiolites and newly obtained Nd-Sr-Pb isotopic data from this study. The isotope data for Evros ophiolite are from Bonev et al. (2023), and for Samothraki ophiolite are from Koglin et al. (2009). The reader is referred to the PDF online for a colour version.

In summary, the Nd-Sr-Pb isotopes systematics revealed mantle-crust interaction caused by mantle wedge magmatic process in the studied Chortiatis magmatic arc-Kassandra-Sithonia back-arc system.

ACKNOWLEDGEMENTS

The support provided by the National Science Fund (Bulgaria) under contract KP-06-N54/5 is greatly acknowledged. We thank both anonymous reviewers for careful reading and commenting on our manuscript, which helped us to improve the final article. We highly appreciate the editorial assistance and comments by Giulio Borghini.

SUPPLEMENTARY MATERIAL

Supplementary data associated with this article can be found in the online version at https://ofioliti.it/index.php/ofioliti/article/view/733

REFERENCES

Anders B., Reischmann T., Poller U. and Kostopoulos D., 2005. Age and origin of granitic rocks of the eastern Vardar zone, Greece: new constraints on the evolution of the Internal Hellenides. J. Geol. Soc. London, 162: 857-870.

Baker J., Peate D., Waight T. and Meyzen C., 2004. Pb isotopic analysis of standards and samples using a 207Pb-204Pb double spike and thallium to correct for mass bias with a double-focusing MC-ICPMS. Chem. Geol., 211: 275-303.

Bébien J., Baroz F., Capedri S. and Venturelli G., 1987. Magmatismes basiques associés à l'ouverture d'un bassin marginal dans les Hellenides internes au Jurassique. Ofioliti, 12: 53-70.

Bonev N. and Filipov P., 2018. From an ocean floor wrench zone origin to transpressional tectonic emplacement of the Sithonia ophiolite, eastern Vardar Suture Zone, northern Greece. Intern, J. Earth Sci., 107: 1689-1711.

Bonev N. and Stampfli G.M., 2003. New structural and petrologic data on Mesozoic schists in the Rhodope (Bulgaria): geodynamic implications. C.R. Geosci. 335: 691-699.

Bonev N. and Stampfli G., 2008. Petrology, geochemistry and geodynamic implications of Jurassic island arc magmatism as revealed by mafic volcanic rocks in the Mesozoic low-grade sequence, eastern Rhodope, Bulgaria. Lithos, 100: 210-233.

Bonev N. and Stampfli G., 2009. Gabbro, plagiogranite and associated dykes in the supra-subduction zone Evros ophiolites, NE Greece. Geol, Mag., 146 (2): 71-92.

Bonev N. and Stampfli G., 2010. Comment on "Geochemistry, petrogenesis and tectonic setting of the Samothraki mafic suite, NE Greece: Trace element, isotopic and zircon age constraints" by N. Koglin, D. Kostopoulos and T. Reischmann [Tectonophysics, 473: 53-68, doi:10.1016/j.tecto.2008.10.028]. Tectonophysics, 483: 413-419.

Bonev N. and Stampfli G., 2011. Alpine tectonic evolution of a Jurassic subduction-accretionary complex: Deformation, kinematics and $^{40}Ar/^{39}Ar$ age constraints on the Mesozoic low-grade schists of the Circum-Rhodope Belt in the eastern Rhodope-Thrace region, Bulgaria-Greece. J. Geodyn., 52:143-167.

Bonev N., Spikings R., Moritz R. and Marchev P., 2010. The effect of early Alpine thrusting in late-stage extensional tectonics: Evidence from the Kulidzhik nappe and the Pelevun extensional allochthon in the Rhodope Massif, Bulgaria. Tectonophysics, 488: 256-281.

Bonev N., Marchev P., Moritz R. and Collings D., 2015a. Jurassic subduction zone tectonics of the Rhodope Massif in the Thrace region (NE Greece) as revealed by new U-Pb and $^{40}Ar/^{39}Ar$ geochronology of the Evros ophiolite and high-grade basement rocks. Gondw. Res., 27: 760-775.

Bonev N., Marchev P., Moritz R. and Filipov P., 2015b. Timing of igneous accretion, composition, and temporal relations of the Kassandra-Sithonia rift-spreading center within the eastern Vardar suture zone, Northern Greece: insights into Jurassic arc/back-arc systems evolution at the Eurasian plate margin. Intern. J. Earth Sci., 104 :1837-1864.

Bonev N., Moritz R., Borisova M. and Filipov P., 2019. Therma-Volvi-Gomati complex of the Serbo-Macedonian Massif, Northern Greece: A Middle Triassic continental margin ophiolite of Neotethyan origin. J. Geol. Soc. London, 176: 931-944.

Bonev N., Dotseva Z. and Chiaradia M., 2023. Nd-Sr-Pb isotopes systematics of the Jurassic Evros ophiolite, eastern Circum-Rhodope Belt, NE Greece. Geol. Mag., 160: 198-205.

Bortolotti V., Chiari M., Marroni M., Pandolfi L., Principi G. and Saccani E., 2013. Geodynamic evolution of ophiolites from Albania and Greece (Dinaric-Hellenic belt): one, two, or more oceanic basins? Intern. J. Earth Sci., 102: 783-811.

Božović M., Prelević D., Romer R.L., Barth M., van den Bogaard P. and Boev B., 2013. The Demir Kapija ophiolite, Macedonia (FYROM): a snapshot of subduction initiation within a back-arc. J. Petrol., 54: 1427-1453.

Brown S.A.M. and Robertson A.H.F., 2003. Sedimentary geology as a key to understanding the tectonic evolution of the Mesozoic-Early Tertiary Paikon Massif, Vardar suture zone, N. Greece. Sedim. Geol., 160: 179-212.

Brown S.A.M. and Robertson A.H.F., 2004. Evidence for Neotethys rooted within the Vardar suture zone from the Voras Massif, northernmost Greece. Tectonophysics, 381: 143-173.

Brun J.-P. and Sokoutis D., 2007. Kinematics of the South Rhodope Core Complex (North Greece). Intern. J. Earth Sci., 96: 1079-1099.

Chiaradia M., Müntener O. and Beate B., 2020. Effects of aseismic ridge subduction on the geochemistry of frontal arc magmas. Earth Planet. Sci. Lett., 531: 115984.

Christofides G., D'Amico C., Del Moro A., Elefteriadis G. and Kyriakopoulos C., 1990. Rb/Sr geochronology and geochemical characters of the Sithonia plutonic complex (Greece). Eur. J. Miner., 2: 79-87.

Christofides G., Koroneos A., Liati A. and Kral J., 2007. The a-type Kerkini granitic complex in North Greece: geochronology and geodynamic implications. Bull. Geol. Soc. Greece. 40: 700-711.

Feinberg H., Edel B., Kondopoulou D. and Michard A., 1996. Implications of ophiolite paleomagnetism for the interpretation of the geodynamics of Northern Greece. In: A. Morris and D.H. Tarling (Eds), Paleomagnetism and tectonics of the Mediterranean region. Geol. Soc. London Spec. Publ., 105: 289-298.

Ferrière J., Baumgartner P.O. and Chanier F., 2016. The Maliac Ocean: the origin of Tethyan Hellenic ophiolites. Intern. J. Earth Sci., 105: 1941-1963.

Hart S.H., 1984. A large-scale isotope anomaly in the Southern Hemisphere mantle. Nature, 309: 753-757.

Himmerkus F., Reischmann T. and Kostopoulos D., 2006. Late Proterozoic and Silurian basement units within the Serbo-Macedonian Massif, northern Greece: the significance of terrane accretion in the Hellenides. In: A.H.F. Robertson and D. Mountrakis (Eds.), Tectonic development of the Eastern Mediterranean Region. Geol. Soc. London Spec. Publ., 260: 35-50.

Himmerkus F., Reischmann T. and Kostopoulos D., 2009a. Serbo-Macedonian revisited: A Silurian basement terrane from northern Gondwana in the Internal Hellenides, Greece. Tectonophysics, 473: 20-35.

Himmerkus F., Reischmann T. and Kostopoulos D., 2009b. Triassic rift-related meta-granites in the Internal Hellenides, Greece. Geol. Mag., 145: 252-265.

Himmerkus F., Zachariadis P., Reischmann T. and Kostopoulos D., 2012. The basement of the Mount Athos peninsula, northern Greece: insights from geochemistry and zircon ages. Intern, J. Earth Sci., 101: 1467-1485.

Ivanova D., Bonev N. and Chatalov A., 2015. Biostratigraphy and tectonic significance of lowermost Cretaceous carbonate rocks

of the Circum-Rhodope Belt (Chalkidiki Peninsula and Thrace region, NE Greece). Creta. Res., 52: 25-63.

Jung D. and Mussallam K., 1985. The Sithonia ophiolite: a fossil oceanic crust. Ofioliti, 10: 329-342.

Kauffmann G., Kockel F. and Mollat H., 1976. Notes on the stratigraphic and paleogeographic position of the Svoula formation in the Innermost Zone of the Hellenides (Northern Greece). Bull, Soc. Géol. Fr., 18: 225-230.

Kockel F., Mollat H. and Walther H.W., 1977. Erläuterungen zur geologischen Karte der Chalkidiki und angrenzender Gebiete 1/100.000 (Nord-Griechenland): Bundes. Geowissen. Rohstoffe, Hannover, 119 pp.

Koglin N., Kostopoulos D. and Reischmann T., 2009. Geochemistry, petrogenesis and tectonic setting of the Samothraki mafic suite, NE Greece: Trace-element, isotopic and zircon age constraints. Tectonophysics, 473: 53-68.

Kydonakis K., Brun J-P., Poujol M., Monié P. and Chatzitheodoridis E., 2016. Inferences on the Mesozoic evolution of the North Aegean from the isotopic record of the Chalkidiki block. Tectonophysics, 682: 65-84.

Macheva L., Peytcheva I., von Quadt A., Zidarov N. and Tarassova E., 2006. Petrological, geochemical and isotope features of Lozen metagranite, Belasitza Mountain-evidence for widespread distribution of Ordovician metagranitoids in the Serbo-Macedonian Massif, SW Bulgaria. Proceed. Annual Conference Bulgaria Geol. Soc. "Geosciences 2006", p. 209-212.

Magganas A.C., 2002. Constraints on the petrogenesis of Evros ophiolite extrusives, NE Greece. Lithos, 65: 165-182.

Magganas A., Sideris C. and Kokkinakis A., 1991. Marginal basin-volcanic arc origin of metabasic rocks of the Circum-Rhodope Belt, Thrace, Greece. Miner. Petrol., 44: 235-252.

McArthur J.M., Howarth R.J. and Bailey T.R., 2001. Strontium isotope stratigraphy: LOWESS version. 3: Best fit for marine Sr-isotope curve for 0-509 Ma and accompanying look-up table for deriving numerical age. J. Geol., 109: 155-170.

Meinhold G., Kostopoulos D., Reischmann T., Frei D. and BouDagher-Fadel M.K., 2009. Geochemistry, provenance and stratigraphic age of metasedimentary rocks from the eastern Vardar suture zone, northern Greece. Palaeo. Palaeo. Palaeo., 277: 199-225.

Mercier J., 1966. Paléogéographie, orogenèse, métamorphisme et magmatisme des zones internes des Hellénides en Macédoine (Grèce): vue d'ensemble. Bull. Soc. Géol. Fr., 7: 1020-1049.

Michail M., Pipera K., Koroneos A., Kilias A. and Ntaflos T., 2016. New perspectives on the origin and emplacement of the Late Jurassic Fanos granite, associated with an intra-oceanic subduction within the Neotethyan Axios-Vardar Ocean. Intern. J. Earth Sci., 105: 1965-1983.

Michard A., Feinberg H. and Montigny R., 1998. Supra-ophiolitic formations from the Thessaloniki nappe (Greece), and associated magmatism: an intra-oceanic subduction predates the Vardar obduction. C.R. Acad. Sci. Paris, 327: 493-499.

Mussallam K., 1991. Geology, geochemistry, and the evolution of an oceanic crustal rift at Sithonia, NE Greece. In: T.J. Peters, A. Nicolas and R.G. Coleman (Eds), Ophiolite genesis and evolution of the oceanic lithosphere. Petrol. Struct. Geol, 5: 685-704, Kluwer, Dordrecht.

Mussallam K. and Jung D., 1986a. Petrology and geotectonic significance of salic rocks preceding ophiolites in the eastern Vardar zone, Greece. Tscherm. Miner. Petrogr. Mitteil., 35: 217-242.

Papanikolaou D., 2009. Timing of tectonic emplacement of the ophiolites and terrane paleogeography in the Hellenides. Lithos, 108: 262-280.

Peytcheva I., von Quadt A., Titorenkova R., Zidarov N. and Tarassova E., 2005. Skrut granitoids from Belassitsa Mountain, SW Bulgaria: constraints from isotope-geochronological and geochemical zircon data. Proceed, Annual Conf. Bulgaria Geol. Soc. "Geosciences 2005", p.109-112.

Ricou L-E., Burg, J-P. Godfriaux I. and Ivanov Z., 1998. The Rhodope and Vardar: the metamorphic and the olistostromic paired belts related to the Cretaceous subduction under Europe. Geodin. Acta, 11: 285-309.

Robertson A.H.F., 2002. Overview of the genesis and emplacement of Mesozoic ophiolites in the Eastern Mediterranean Tethyan region. Lithos, 65: 1-67.

Robertson A.H.F. and Dixon J.E., 1984. Introduction: aspects of the geological evolution of the Eastern Mediterranean. In: Robertson A.H.F. and Dixon J.E., (Eds), Tectonic evolution of the Eastern Mediterranean. Geol. Soc. London Spec. Publ., 17: 1-74.

Robertson A.H.F. Dixon J.E., Brown S., Collins A., Morris A., Pickett E., Sharp I. and Ustaömer T., 1996. Alternative tectonic models for the Late Palaeozoic-Early Tertiary development of Tethys in the Eastern Mediterranean region. In: A. Morris and D.H. Tarling (Eds.), Paleomagnetism and tectonics of the Mediterranean Region. Geol. Soc. London Spec. Publ., 105: 239-263.

Robertson A.H.F. Trivić B., Đerić N. and Bucur I.I., 2013. Tectonic development of the Vardar Ocean and its margins: Evidence from the Republic of Macedonia and Greek Macedonia. Tectonophysics, 595-596: 25-54.

Rollinson H., 1993. Using geochemical data: evaluation, presentation, interpretation. John Wiley and Sons, Tottenham, 343 pp.

Saccani E., Beccaluva L., Photiades A. and Zeda O., 2011. Petrogenesis and tectono-magmatic significance of basalts and mantle peridotites from the Albanian-Greek ophiolites and sub-ophiolitic mélanges. New constraints for the Triassic-Jurassic evolution of the Neo-Tethys in the Dinaride sector. Lithos, 124: 227-242.

Saccani E., Bortolotti V., Marroni M., Pandolfi L., Photiades A. and Principi G., 2008. The Jurassic association of backarc basin ophiolites and calc-alkaline volcanics in the Guevgueli complex (Northern Greece): implications for the evolution of the Vardar zone. Ofioliti, 33: 209-227.

Schmid S.M., Bernoulli D., Fügenschuh B., Matenco L., Schefer S., Schuster R., Tischler M. and Ustaszewski K., 2008. The Alpine-Carpathian-Dinaridic orogenic system: correlation and evolution of tectonic units. Swiss J. Geosci., 101: 139-183.

Smith A.G., 1993. Tectonic significance of Hellenic-Dinaric ophiolites. In: H.M. Prichard, T. Alabaster, N.B.W. Harris and C.R. Neary (Eds.), Magmatic process and plate tectonics. Geol. Soc. London Spec. Publ.,76: 213-243.

Spray J.G., Bébien J., Rex D.C. and Roddick J.C., 1984. Age constraints on the igneous and metamorphic evolution of the Hellenic-Dinaric ophioites. In: A.H.F. Robertson and J.E. Dixon (Eds.), Tectonic evolution of the Eastern Mediterranean. Geol. Soc. London Spec. Publ., 17: 619-627.

Stampfli G.M., 2000. Tethyan oceans. In: E. Bozkurt, J.A. Winchester and J.D.A., Piper (Eds.), Tectonics and magmatism in Turkey and surrounding region. Geol. Soc. London Spec. Publ., 173: 1-23.

Stampfli G.M. and Borel G.D., 2002. A plate tectonic model for the Paleozoic and Mesozoic constrained by dynamic plate boundaries and restored synthetic oceanic isochrons. Earth Planet. Sci. Lett., 196: 17-33.

Stampfli G.M. and Borel G.D., 2004. The TRANSMED transects in space and time: constraints on the paleotectonic evolution of the Mediterranean domain. In: W. Cavazza, F. Roure, W. Spakman, G.M. Stampfli and P. Ziegler (Eds.), The TRANSMED Atlas: the Mediterranean Region from Crust to Mantle. Springer Verlag, Berlin, p. 53-90.

Stampfli G.M. and Hochard C., 2009. Plate tectonics of the Alpine realm. In: J.B Murphy, J.D. Keppie and A.J. Hynes (Eds.), Ancient orogens and modern analogues. Geol. Soc. London Spec. Publ., 327: 89-111.

Sun S.S. and McDonough W.F., 1989. Chemical and isotopic systematics of ocean basalts: implications for mantle composition and processes. In: A.D. Saunders and M.J. Norry (Eds.), Magmatism in ocean basins. Geol. Soc. London Spec. Publ., 42: 313-345.

Tanaka T., Togashi S., Kamioka H., Amakawa H., Kagami H., Hamamoto T., Yuhara M., Orihashi Y., Yoneda S., Shimizu H., Kunimaru T., Takahashi K., Yanagi Y., Nakano T., Fujimaki H., Shinjo R., Asahara Y., Tanimizu M. and Dragusanu C., 2000. JNdi-1: a neodymium isotopic reference in consistency with La Jolla neodymium. Chem. Geol., 168: 279-281.

Turpaud P. and Reischmann T., 2010. Characterization of igneous terranes by zircon dating: implications for UHP occurrences and suture identification in the Central Rhodope, northern Greece. Intern. J. Earth Sci., 99: 567-591.

Zachariadis P., 2007. Ophiolites of the eastern Vardar zone, N. Greece. Ph.D. thesis, 131 pp., Univ. Mainz, Germany.

Zachariadis P., Kostopoulos D., Reichmann T., Himmerkus F., Matukov D. and Sergeev S., 2006. U-Pb ion-microprobe zircon dating of subduction-realted magmatism from northern Greece: The ages of the Guevgueli, Thessaloniki and Chalkidiki igneous complexes. Geophys. Res. Abstr. 8, paper EGU06-A-05560.

Zindler A. and Hart S.R., 1986. Chemical geodynamics. Ann. Rev. Earth Planet. Sci., 14: 493-571.

Received, January 16, 2024
Accepted, April 21, 2024